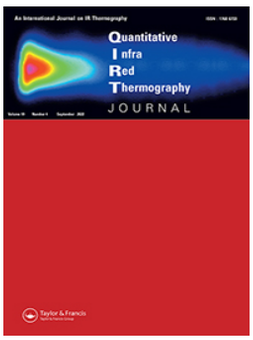

Quantitative InfraRed Thermography Journal

ISSN: (Print) (Online) Journal homepage: https://www.tandfonline.com/loi/tqrt20

MMSHRs: a morphology model of suspicious hyperthermic regions for degree of severity prediction from breast thermograms

Usha Rani Gogoi, Mrinal Kanti Bhowmik & Gautam Majumdar

To cite this article: Usha Rani Gogoi, Mrinal Kanti Bhowmik & Gautam Majumdar (2022): MMSHRs: a morphology model of suspicious hyperthermic regions for degree of severity prediction from breast thermograms, Quantitative InfraRed Thermography Journal, DOI: 10.1080/17686733.2022.2097614

To link to this article: https://doi.org/10.1080/17686733.2022.2097614

QUANTITATIVE INFRARED THERMOGRAPHY JOURNAL
https://doi.org/10.1080/17686733.2022.2097614

Taylor & Francis
Taylor & Francis Group

MMSHRs: a morphology model of suspicious hyperthermic regions for degree of severity prediction from breast thermograms

Usha Rani Gogoi[a], Mrinal Kanti Bhowmik[a] and Gautam Majumdar[b]

[a]Department of Computer Science & Engineering, Tripura University (A Central University), Suryamaninagar, Tripura, India; [b]Department of Radiotherapy, Atal Bihari Vajpayee Regional Cancer Centre, Agartala Govt. Medical College, Agartala, Tripura, India

ABSTRACT

The presence of suspicious hyperthermic regions (SHRs) in breast thermograms is a prominent indicator of breast pathology, for which delineation and analysis of SHRs have a crucial role in early detection of breast abnormalities. A novel approach for breast abnormality grading, namely the morphology model of suspicious hyperthermic regions (MMSHRs), is proposed here. The proposed model first segments SHRs from breast-thermograms and then analyzes their morphology to grade the thermograms according to their degree of severity. To segment SHRs, a simple but effective method that computes the similarity score of each pixel with the highest intensity value is designed. . The performance of the proposed segmentation method is tested on both public and in-house-captured datasets. With the optimal values of seven evaluation metrics, the proposed segmentation method outperforms other state-of-the-art segmentation methods. The values of evaluation metrics further justify that the proposed SHRs segmentation method addresses all the limitations regarding infrared breast thermogram segmentation, and reduces the under-segmentation and over-segmentation of SHRs. Following segmentation of SHRs, the MMSHRs extract the corresponding morphological features, allowing the classification of thermograms into mild and severely abnormal with the classification accuracy of 91% and area under the receiver operating characteristic curve of .9998.

ARTICLE HISTORY
Received 21 July 2021
Accepted 30 June 2022

KEYWORDS
Breast cancer; degree of severity; infrared breast thermography; morphological features; suspicious hyperthermic regions

1. Introduction

Breast cancer is the principal cause of cancer-related deaths among women globally, but the risk of death can be reduced if the cancer is detected and diagnosed early [1]. Owing to the lack of breast screening modalities in younger age groups, it has been reported that only 0% and 1.9% of diagnoses were possible under the age groups of 20 and 20–34 years, respectively [2]. In India, over the last few decades, the average age of breast cancer development has shifted to 30–40 years [3]. With the vulnerability of younger women to the advancement of cancer tumours [4] and the radiation risk of X-ray mammography (MG) [5–7], the demand for a radiation-free breast imaging modality is increasing for early

CONTACT Mrinal Kanti Bhowmik mrinalkantibhowmik@tripurauniv.ac.in Department of Computer Science & Engineering, Tripura University (A Central University), Suryamaninagar, Tripura, India

detection of breast abnormalities in asymptomatic subjects. Infrared breast thermography (IBT) has become a potential tool for the early detection of breast abnormalities because it is radiation-free, non-invasive, and has a sensitivity of 90% [8]. Being a functional imaging modality, IBT can capture the temperature emitted by the skin overlying a malignancy [9,10]. The increased rate of blood flow and metabolic activity to supplement the growth of a tumour cause increased regional surface temperature of the breast, which appears as higher temperature regions known as suspicious hyperthermic regions (SHRs) in breast thermograms [11–14]. In literature, it has been reported that in comparison to the thermograms with asymmetric thermal patterns, those exhibiting increased nipple temperature, SHRs, and vascular changes may be more suspicious and indicate more severe breast problems [11–14]. Moreover, the aggressiveness and prognosis of tumours directly influence the thermovascular activities in breasts [4]. Hence, to assess the physiological state of breasts, analysis of SHRs may be significant. Additionally, by analysing SHRs, it is possible to predict and grade the degree of severity in breast thermograms.

While designing an SHRs based breast abnormality grading system, it is apparent that the accuracy of the SHRs analysis entirely depends on the efficient segmentation of the SHRs. Although several approaches for the segmentation of medical images have been reported in the literature, most of these state-of-the-art segmentation methods are image and application-dependent. Hence, their results are highly dependent on the corresponding image characteristics. Moreover, segmentation of SHRs from breast thermograms is a difficult task because of the complexity and diversity of thermal images like there is no clear boundary between an SHR and the surrounding region, poor contrast, variation in shape and size of SHRs, and locality variation of SHRs, etc. Each of these limitations of thermograms is detailed below.

1.1. Lack of clear edges and intensity overlapping

Like the visual images, the thermal images do not contain clear edges. A medical thermal image visually represents the surface temperature distribution of a human body, for which there is a smooth transition of temperature values from one region to another. The intensity values mapped from the temperature values also maintain the property of smooth transition in the corresponding thermal images. Because of this smooth transition, no sharp discontinuity is present between the regions, making it tedious to separate one region from others. As a result, thermal images are blurry with no clear edges. The smooth transition also introduces the concept of pixel overlapping, where the boundary pixels, that is pixels at the edge of two regions have the characteristics of two regions. Because, different regions in a thermal image are represented with various pseudo colours, the edge pixels have intensity values close to both regions. Therefore, the segmentation of thermogram is a challenging task.

1.2. No definite location of SHRs

The presence of an SHR in a breast thermogram is the most significant marker of breast abnormality. However, SHRs are not always confined to a fixed location and may appear in more than one location of a thermogram. In addition, SHRs are not sufficiently compact; they blow out over a region. Although every SHR within a breast area have equal importance, sometimes they do not possess the same intensity values, making some segmentation methods ineffective for extracting all SHRs accurately. This may result in a missed segmentation.

1.3. No definite shape of SHRs

The SHRs of a thermogram are unique in that the SHRs of two consecutive thermograms for the same patient taken seconds apart do not appear exactly the same. Moreover, SHRs do not bear any regular shape, for which drawing conclusion based on shape analysis is complicated.

Because of these limitations of IBT, very few studies [15,16] have addressed the extraction of SHRs for the analysis of breast thermograms. Existing segmentation methods for SHRs comprise clustering-based [17–27], deformable model-based [17,27], threshold-based [28,29] and region-based segmentation methods [28,29]. Table 1 summarises the state-of-the-art segmentation methods. As listed in Table 1, the datasets used for the extraction of SHRs are very small in almost all studies, except that by Pramanik et al. [27]. Moreover, no report on quantitative evaluation of segmentation errors, such as under-segmentation (USeg) and over-segmentation (OSeg) rates of state-of-the-art segmentation methods, were found in the literature review. Thus, the adoption of a particular

Table 1. The summary on SHRs segmentation methods.

Segmentation techniques	No. of images used	Method used	Limitations
Clustering based method [17–27]	30, 6, 4, 15, 20, 14, NP, 34, 12, 20, 74Ab	K-means, fuzzy c-means, mean-shift (MS), Expectation Maximization (EM), particle swarm optimisation	• Initialisation of cluster number • Initialisation of cluster center • Selection of parameters (e.g. bandwidth in MS) • Sometimes long computational time.
Deformable model based method [17,27]	30, 74Ab	Level set (LS) method	• Initial placement of contour, embedding of the object and gaps in the boundaries [21] • Construction of appropriate velocities for advancing the LS function
Threshold based method [28,29]	40 images, DBT-TU-JU [29]: 40 & DMR [30]: 22	Thresholding method	• Selection of threshold value • Not consider the spatial details • Improper selection of threshold may increase over-segmentation and under-segmentation
Region based method [28,29]	44 images, DBT-TU-JU [29]: 40 & DMR [30]: 22	Region shrinking (RASIT), region growing	• Manual selection of seed points, • Selection of stopping criteria, • Noise and variation of intensity results in holes or oversegmentation

*Ab – Abnormal, NP – Not provided, RASIT - Region shrinking based accurate segmentation of inflammatory areas from thermograms.

method for SHR extraction is challenging. The literature survey clearly supports the fact that no work has been conducted to grade abnormality in breast thermograms to date. Several works [15] differentiated thermograms into malignant and benign groups by analysing SHRs. However, categorisation of thermograms into benign and malignant solely based on findings from thermograms is not convenient as IBT is just functional imaging and cannot provide any structural information. Rather, grading the abnormality of thermograms as mild abnormal (MA) and severely abnormal (SA) by analysing the SHRs is more convenient and will allow subjects having SA thermograms to seek doctor's attention for further evaluation of their breast health.

Since SHRs are only defined through the intensity value changes related to the surrounding intensity values, developing an automated and efficient SHRs segmentation method is technically challenging. Furthermore, owing to the variation in metabolic activities across patients, the size, structure, and location of SHRs considerably vary, which in turn prohibits the use of prior knowledge on components such as shape and location in segmentation.

Considering the limitations of existing systems, this research focuses on the development of a novel breast abnormality grading system for rapidly identifying asymptomatic patients that need urgent medical attention which will thus, help in the early detection of breast abnormalities. The proposed morphology model of SHRs (morphology model of suspicious hyperthermic regions – MMSHRs) comprises two major parts: the first addresses the automatic segmentation of SHRs from breast thermograms and the second analyzes the morphology of the extracted SHRs to predict the degree of severity in thermograms. Since the efficiency of the grading system depends on the accuracy of the segmentation results; the proposed segmentation method attempts to address the segmentation challenges of IBT. In addition, the proposed segmentation method attempts to reduce OSeg and USeg error. Figure 1 presents the overview of the proposed system. The motivation of the method is to use the fact that SHRs have the highest intensity value for which SHRs can be efficiently detached from the remaining portion of breast thermograms. Based on this key idea, if the contrast of the intensity value of a pixel with the highest intensity value of an SHR is very small, then it has a higher chance of belonging to the SHR; in contrast, if the contrast is sufficiently large, then the pixel belongs to a non-SHR in the image.

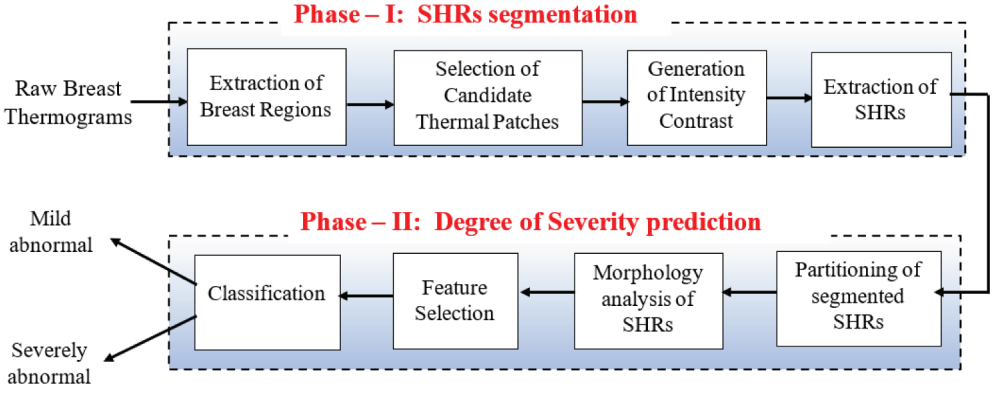

Figure 1. Flow of the MMSHRs.

The remainder of the paper is divided as follows. The proposed SHRs segmentation method is described in Section 2. Section 2 also presents the morphological analysis of the segmented SHRs to predict the degree of severity. Details of the experimental datasets and extensive experiments performed for the evaluation of the proposed MMSHRs system are provided in Section 3 and Section 4 respectively. Section 5 discusses the advantages and limitations of the proposed MMSHRs system. Finally, the paper ends with the conclusion in Section 6.

2. Proposed methodology

2.1. Stage 1 – segmentation of SHRs

This section describes the proposed SHRs segmentation method for predicting the severity of breast abnormalities. In breast thermograms, SHRs exhibit higher temperature values for which their mapping to the intensity scale also has higher intensity values. The proposed method comprises four steps: First, the breast region (BR) is extracted by using a semi-automatic segmentation method, followed by normalisation of the segmented images to identify the candidate thermal patches (CTPs) corresponding to SHRs. Third, the similarity score of each image pixel with the highest intensity value is computed. Finally, the output of the third step is binarized to extract SHRs from breast thermograms. These steps are described in detail in the following subsections.

2.1.1. Pre-processing of breast thermograms

As authors intend to segment SHRs within the BR of a thermogram, the extraction of BRs prior to SHRs segmentation is crucial. Therefore, at first, the BR from a raw breast thermogram in the 'Rainbow HC' colour pallet was extracted using a semi-automatic BR segmentation algorithm, as discussed in [30]. This algorithm requires human intervention to select the lower parabolic curves of both breasts. Then, using the manually selected curves, the segmentation algorithm creates a breast mask for each individual thermogram, the convolution of which extracts the BR.

The SHRs in breast thermograms characteristically contrast their surrounding regions in colour and intensity (as illustrated in Figure 2(a)), and thus can be used as important factors for separating SHRs from the surrounding areas. The original RGB breast thermograms constitute red, green, and blue channels. Unlike the red and green channels, the contrast between SHRs and non-SHRs is high in the blue channel, as shown in Figure 2(d). Hence, instead of using the RGB image, the blue channel image, I_b of a thermogram is

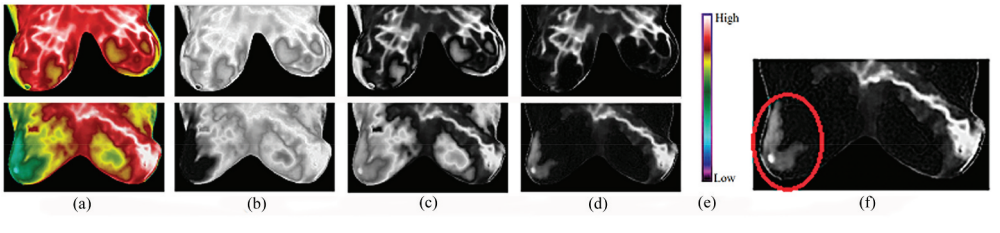

Figure 2. (a) segmented BRs, (b) red channel, (c) green channel, (d) blue channel image, (e) temperature scale, (f) low-temperature regions in blue channel, circled in red.

selected for SHRs segmentation. However, the variation in the dynamic range of I_b from different breast thermograms necessitates the normalisation of these images in the range of [0–255] prior to the extraction of SHRs. The normalisation procedure for I_b is detailed in Algorithm-1. Figure 2(a) illustrates the results of BR segmentation in some sample breast thermograms.

2.1.2. Selection of candidate thermal patches

This step attempts to identify all possible thermal patches that may be considered as SHRs. As shown in Figure 2(f) , along with the higher temperature regions, some lower temperature regions, which are marked with a red circle and represented by the green-blue pseudo-colour in RGB breast thermograms (please refer to the *Temperature Scale* shown in Figure 2(e)), are also apparent in I_b. Hence, for the accurate segmentation of SHRs, the selection of CTPs is crucial. For this, the corresponding red channel image I_r is used as I_r does not contain the

Algorithm 1: Image Normalization

Input: Image I_b / I_r

Output: Normalized Image I_b' / I_r'

Phase1: Find the Intensity range of all Image (I_b / I_r)

For i = 1 to Number of images *(N)*

$\max(i) \leftarrow$ maximum of I_b^i

$\min(i) \leftarrow$ minimum of I_b^i

end

$new\_max \leftarrow \underset{i=1\ to\ N}{\text{maximum}}\{\max(i)\}$

$new\_min \leftarrow \underset{i=1\ to\ N}{\text{minimum}}\{\min(i)\}$

Phase2: Normalization of image (I_b / I_r)

$diff \leftarrow new\_max - new\_min$

$max \leftarrow$ maximum of I_b

$min \leftarrow$ minimum of I_b

$$I_b' \leftarrow (I_b - min)\left[\frac{diff}{max - min}\right] + new\_min$$

green-blue pseudo colour components of the RGB image as depicted in Figure 2(b), owing to the absence of the red component. However, before using I_r for filtering out the lower temperature regions or non-CTPs from I_b', the I_r images are also normalised to the range of [0–255]. The procedure detailed in Algorithm-1 was used to normalise the I_r images.

After normalising I_r, the green-blue shade of pseudo colour in RGB thermograms is represented by the intensity value [0–70] in the I_r' image. Hence, using a threshold-based method as illustrated in Equation (1), the regions with intensity values less than I_{Thresh} in I_r' are discarded from I_b' and those with intensity values higher than I_{Thresh} in I_r' are maintained in I_b' and considered as the CTPs.

$$I_b'(i,j) = \begin{cases} I_b'(i,j), & \text{if } I_r'(i,j) > I_{Thresh} \\ 0, & \text{if } I_r'(i,j) < I_{Thresh} \end{cases} \tag{1}$$

Here, the value of I_{Thresh} is 70.

2.1.3. Generation of intensity contrast map based on similarity score

In thermal images, because of the absence of a sharp transition of intensity values from one region to others, the boundaries of the CTPs are indistinct, and there is a smooth transition of boundary pixels. Hence, to decide if these boundary pixels belong to the SHRs, an intensity contrast map (ICM), ϕ was generated based on the key idea of similarity between intensity values of the CTPs and the highest intensity value. Each entry of ϕ is the similarity score of each intensity value with the highest intensity value. As eachI'_b is normalised in the dynamic range of [0–255], the maximum intensity value δ in eachI'_b is 255. Then, this maximum intensity value is used to generate ϕ by finding the difference between each squared intensity value and δ^2 as given in Equation (2)).

$$\begin{aligned}\phi_{ij} &= diff((I'_b)_{ij}, \delta) \\ &= \sqrt{(I'_b)_{ij}^{\,2} - \delta^2}, \qquad (i,j) \in I'_b\end{aligned} \tag{2}$$

Thus in ϕ, the contrasts of pixels with higher intensity values were found to be very small, whereas the contrasts were larger for pixels with lower intensity values. In the ICM, to represent the lower difference values as higher similarity scores and larger differences with lower similarity scores, the ϕ *is* complemented. The complemented ICM matrix, ϕ_c resembles with $I'_b$and highlights the SHRs in the breast thermogram. Figure 3(d) presents ϕ_c of some sample breast thermograms bearing SHRs (Figure 3(a,b)).

2.1.4. Extraction of suspicious hyperthermic regions

For further analysis of the degree of severity in breast thermograms, instead of similarity score values, the actual intensity values of the SHRs are required. Hence, to obtain the intensity values corresponding to the high similarity score of ϕ_c, a binary mask is created from ϕ_c using Otsu's thresholding method, which chooses a threshold by minimising the interclass variance between the black and white pixels [32]. Then, the generated binary masks are convolved with the corresponding RGB images, I to obtain the SHRs, I_{hs} of the breast thermograms. The binary masks and segmented SHRs of some sample breast thermograms are displayed in Figure 3(e–g), respectively. The corresponding ground truth (GT) images of the SHRs are illustrated in Figure 3(f).

2.2. Stage 2 – degree of severity prediction

The second stage of the proposed method aims to categorise SHRs into MA and SA thermograms by predicting the degree of severity of the SHRs. For this purpose, the dynamic range of each extracted SHR was normalised to the range of [0–255]. To predict the degree of severity, some morphological characteristics of these SHRs were critically analysed. This stage involved three steps.

2.2.1. Partitioning of segmented SHRs

To analyse the segmented SHRs, the intensity values of each SHR are further partitioned into k levels, hs_i, $i = 1$ to k such that each partition contains intensity values in the range of [(*i-1)*L*, (*i*L)*-1]. Based on the trial-and-error method, authors found that having $L = 50$ grey

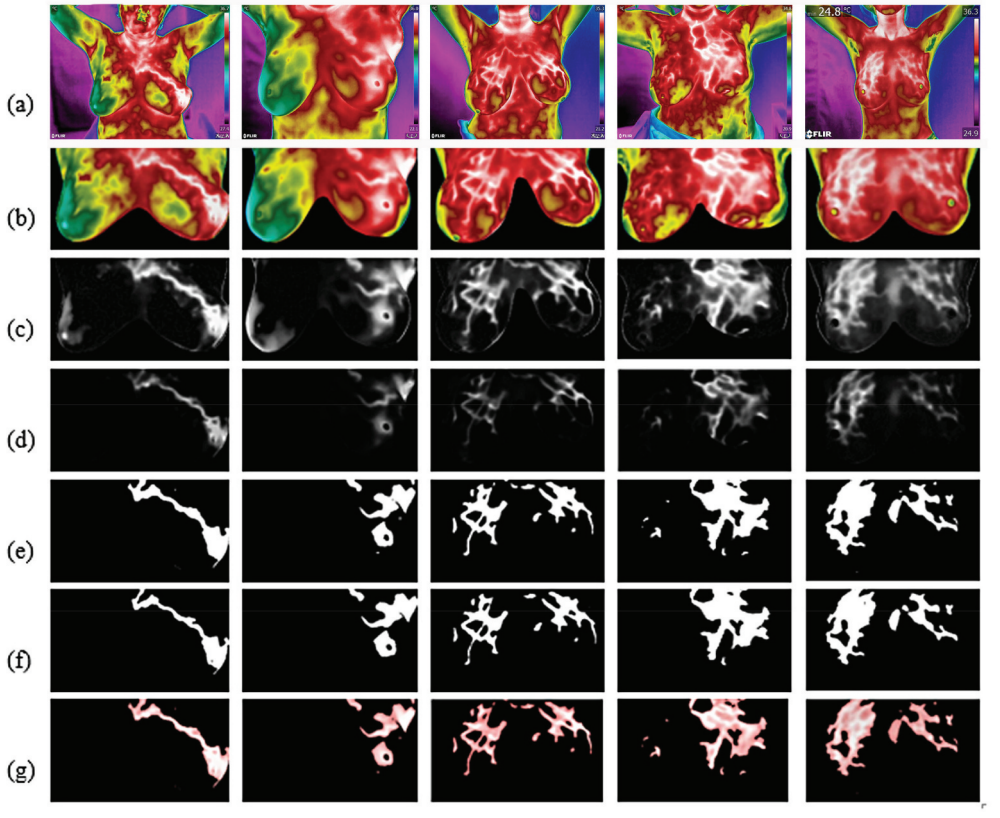

Figure 3. (a) original breast thermograms, (b) segmented BRs, (c) blue channel images, (d) intensity contrast maps, (e) binary masks, (f) ground truth images and (g) suspicious hyperthermic regions.

levels in each partition is optimal for morphology-based SHRs analysis. As the dynamic range of an image containing SHRs is [0-255], so the value L = 50 produces $k = 5$ hot regions within the segmented I_{hs}.

The partitioning of each SHR was obtained by applying the Algorithm-2 and Figure 4 illustrates the partitioning of SHRs of a MA and a SA breast thermogram. It is apparent in Figure 4 that the first hot region hs_1 of the SA thermogram is considerably larger than that

Algorithm 2: Partitioning of Segmented SHRs

Input: The Segmented Hyperthermic Regions I_{hs}, cluster range L
Output: The clustered images hs_i, $i = 1 \ldots\ldots k$

```
1.  Inhs ← Normalize His
2.  Set range ← L;
3.  Ihs ← floor[Inhs / range]
4.  for i = 1: maximum (Ihs)
        if Ihs = = i
            hsi ← set of all pixels of Ihs whose values is i as 1 and
                  remaining 0
            hsi ← multiply hsi with Inhs
        end if
    end for
```

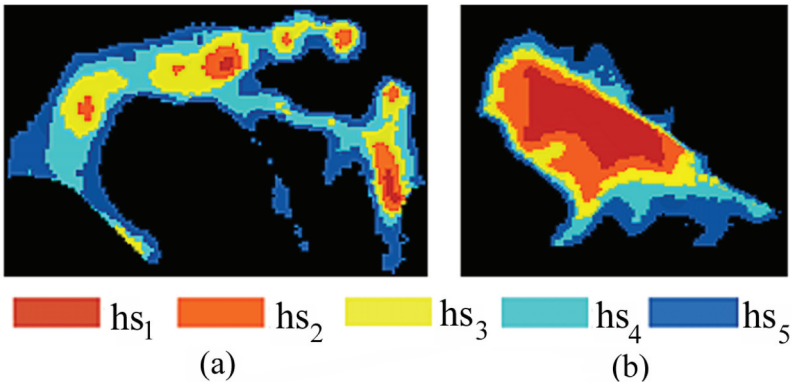

Figure 4. Clustering output of (a) mild abnormal and (b) severely abnormal breast thermograms.

of the MA thermogram. Similarly, the second hot region hs_2 of the SA thermogram is considerably larger than that of the MA thermogram. In contrast, in the MA thermograms, the lower temperature (intensity) regions, that is, hs_3, hs_4 and hs_5 are considerably larger than those in the SA thermograms. Based on these key characteristics of the SHRs in MA and SA thermograms, a feature-based analysis of these segmented SHRs could be performed.

2.2.2. Morphology of SHRs

For morphological analysis of the SHRs, the hot regions hs_i and hs_j are added together, where the pixel values of hs_i are higher than those of hs_j and these merged regions are denoted as HS_i, where $i = 1$ to 5. Thus, each evolving region encompasses the previous regions, as demonstrated in Equations (3)–(7). When two subsequent hot regions merge, they start sharing the same characteristics.

$$HS_1 = hs_1 \tag{3}$$

$$HS_2 = hs_1 \cup hs_2 \tag{4}$$

$$HS_3 = hs_1 \cup hs_2 \cup hs_3 \tag{5}$$

$$HS_4 = hs_1 \cup hs_2 \cup hs_3 \cup hs_4 \tag{6}$$

$$HS_5 = hs_1 \cup hs_2 \cup hs_3 \cup hs_4 \cup hs_5 \tag{7}$$

For each HS_i, a set of four shape features are computed as follows:

- Area: Actual number of pixels in each HS_i.
- Equivalent diameter (*ED*): Diameter of a circle with the same area as region HS_i
- Convex area (*CA*): Area of the smallest region that is convex and contains the original HS_i

- Fractal dimension (*FD*): This measures the complexity of an object as the ratio of *log(B)* to *log(r)*, where *B* is the number of boxes that cover HS_i and *r* is the magnification or inverse of the box size [33,34].

In addition to the four features discussed above, another feature named relative suspicious area (*RSA*) is computed to characterise the SHRs of MA and SA thermograms, as follows:

- Relative Suspicious Area is the ratio of the number of pixels with intensity values ≥150, to the number of pixels with intensity values <150 given by:

$$RSA = \frac{hs_1 + hs_2}{hs_3 + hs_4 + hs_5} \tag{8}$$

2.2.3. Designing classifiers

To predict the degree of abnormality based on the computed feature values and to differentiate the thermograms into MA and SA categories, authors used the support vector machine (SVM). This choice of using SVM was motivated by the experimental findings of the works [11,30], where SVM exhibited the best classification performance among different classifiers. The SVM is the most widely used supervised learning method for classification. It can minimise the empirical classification error and maximise the geometric margin that maximises the class separation [34]. The performance of SVM with three different kernels [12]: i) Gaussian radial basis function (SVM_R), ii) linear (SVM_L), and iii) polynomial (SVM_P) were explored to obtain the best classification accuracy. Except for the linear kernel, the parameters of the other two kernels were altered to obtain better classification accuracy.

3. Experimental setup

To assess the performance of the proposed MMSHRs, the presence of a sufficiently large GT annotated breast thermogram database is crucial. However, as reported in [29], only one publicly available breast thermogram database, the Database of Mastology Research (DMR) [35], has been found in the literature to date. It is an unbalanced dataset with 240 samples of healthy subjects and 47 samples of unhealthy subjects and does not contain the GT images of SHRs. Therefore, considering all of these factors it is imperative to design a GT-annotated breast thermogram database. However, IBT is very sensitive to environmental changes, which may reduce the potential of IBT in early breast cancer detection, leading to the standardisation of the breast thermography procedure [13,29]. Hence, to acquire thermograms, a standard acquisition protocol suite has been designed [29] comprising a number of important parameters: patient preparation, patient acclimation, patient intake form, examination room condition, patient position, and acquisition views. Breast thermograms were acquired using a FLIR T650sc thermal camera with thermal sensitivity of <20mK @ 30°C and image resolution of 640 px x 480 px. The name of the designed database is the Department of Biotechnology-Tripura University-Jadavpur University (DBT-TU-JU) breast thermogram database. To validate the images of the DBT-TU-JU database, the database was also annotated with the findings of clinical breast

examination (CBE), X-ray mammography (MG), and fine-needle aspiration cytology (FNAC) (if available) of each subject undergoing IBT. For almost all cases, the results of all examinations (CBE, MG, and FNAC) were in agreement with the findings of the IBT analysis. In addition, the DBT-TU-JU database was also annotated with the GT images of the SHRs generated by four medical experts, which enables the researchers to measure the effectiveness of their proposed SHRs segmentation algorithms. The procedure for generating the GT images of breast thermograms from the DBT-TU-JU database is detailed in [29].

Two datasets, D1 and D2 were formed corresponding to the in-house acquired DBT-TU -JU breast thermogram database [29] and the publicly available DMR database [30] respectively. The D1 dataset comprises 70 SHRs bearing breast thermograms, whereas the D2 dataset consists of 30 SHR bearing breast thermograms. Because the GT images of the DMR are not available, the authors received help from medical experts to generate the GT images.

As the proposed method involves two stages, the evaluation was performed at two levels. First, the performance of SHR segmentation in every thermogram was evaluated using the provided GT images. For efficient abnormality grading, the segmentation performance must be as high as possible, because the number of pixels detected as SHR is crucial for predicting the degree of severity in thermograms. To evaluate the performance of the segmentation stage, a set of the five most widely used supervised evaluation metrics, namely, the Dice similarity coefficient (DSC) [36,37], Jaccard index (JI) [37], precision (Pr) [38], recall (Rc) [38] and root mean square (RMS) [39] were used. Values of DSC, JI, Pr and Rc closer to 1 indicate better segmentation quality, whereas values closer to 0 indicate poor segmentation. In contrast, RMS values closer to 0 indicate better segmentation, and values closer to 1 indicate poor segmentation. The first four evaluation metrics are commonly known as spatial-overlap-based metrics as they are based on four basic cardinalities: true positive (TP), true negative (TN), false positive (FP), and false negative (FN), each of which measures the amount of overlapping or any missed area between the segmentation result and the binary GT. Regarding segmentation, the TP, TN, FP, and FN are defined as follows: TP is the number of SHR pixels correctly detected as SHR pixels, TN is the number of non-SHR pixels correctly detected as non-SHR pixels, FP is the number of non-SHR pixels falsely detected as SHsR pixels; FN is the number of SHR pixels falsely detected as non-SHR pixels.

In addition, the quality of segmentation is measured by quantifying the USeg and OSeg of the segmented outputs. USeg and OSeg occur when the segmented SHR is larger and smaller than the annotated GT image respectively, as shown in Figure 5(a). For the computation of USeg and OSeg, the work of M. Belgiua, and L. Drăguţb [40] was followed. The computation of these seven evaluation metrics is followed by the computation of these metrics from other state-of-the-art segmentation methods to make a comparative study of the proposed segmentation method.

The second level of evaluation is very important in perspective of breast screening because it evaluates the performance of the second phase of the MMSHRs in differentiating the MA thermograms from the SA thermograms. Categorisation of abnormal thermograms based on the combined report of clinical examination, patient symptoms, MG and FNAC findings is considered the gold standard for evaluation. Abnormal thermograms of subjects whose MG or FNAC show the presence of either benign or malignant tumours are

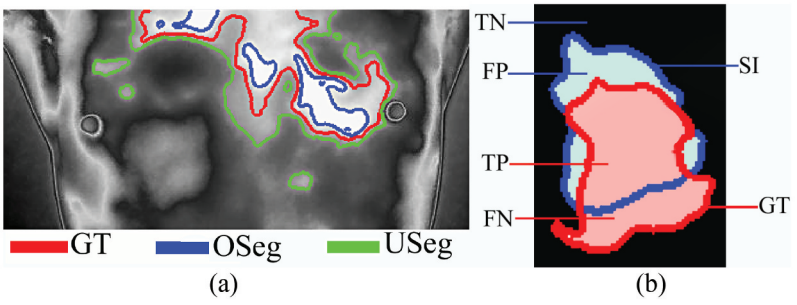

Figure 5. (a) sample breast thermogram showing the GT, OSeg and USeg regions of an SHR; (b) TP, TN, FP and FN regions of a SHR with respect to a GT image and a segmented image.

labelled as SA thermograms. In contrast, abnormal thermograms whose FNAC reports are not available and MG could not reveal the presence of any tumour or calcification but are found to be abnormal clinically, or the corresponding subjects are suffering from several breast problems including blood discharge, pus formation, the presence of lumps for a long period of time are labelled as MA. However, in the DMR, thermograms are not categorised as MA or SA; they are categorised as either 'sick' or 'healthy'. Moreover, some subjects in the healthy group, suffer from breast problems, and their thermograms reveal the presence of abnormality through SHRs. For evaluation purposes, the authors considered these healthy thermograms as MA thermograms because they are suffering from some minor breast problems and the thermograms of 'sick' subjects are considered SA thermograms. However, because the experimental DMR dataset was small, the thermograms of both the DBT-TU-JU and the DMR were combined to evaluate the screening phase of the proposed MMSHRs method. The diagnostic performance of the proposed model was evaluated by computing the five most widely used performance indices: accuracy (Acc), sensitivity (Se), specificity (Sp), positive predictive value (PPV) and negative predictive value (NPV).

All the experiments were performed in a system with moderate hardware specifications, including a 64 bit Windows 10 OS, Intel® i3-Core™ processor, and 4 GB of RAM. To implement the MMSHRs, the MATLAB 2015 interface was employed.

4. Experimental results

4.1. SHRs segmentation phase

A qualitative comparison of the segmentation results of the MMSHRs with the GT images and the output of other state-of-the-art SHR segmentation methods is shown in Figure 6. To achieve an unbiased comparison of the SHR segmentation methods, the optimal cluster number or optimal window size for the clustering methods (EM, FODPSO, KMC, FCM, MS) was selected based on the I-index [41] value, which is known as a cluster validity index. Figure 6(a) shows sample breast thermograms, with the corresponding GT images of the SHRs of the DBT-TU-JU dataset in Figure 6(b). Comparing the shapes of the segmented SHRs of the proposed method (Figure 6(c)) with the GT images proved that the proposed method can extract the exact shapes of SHRs. In contrast, KMC and FCM

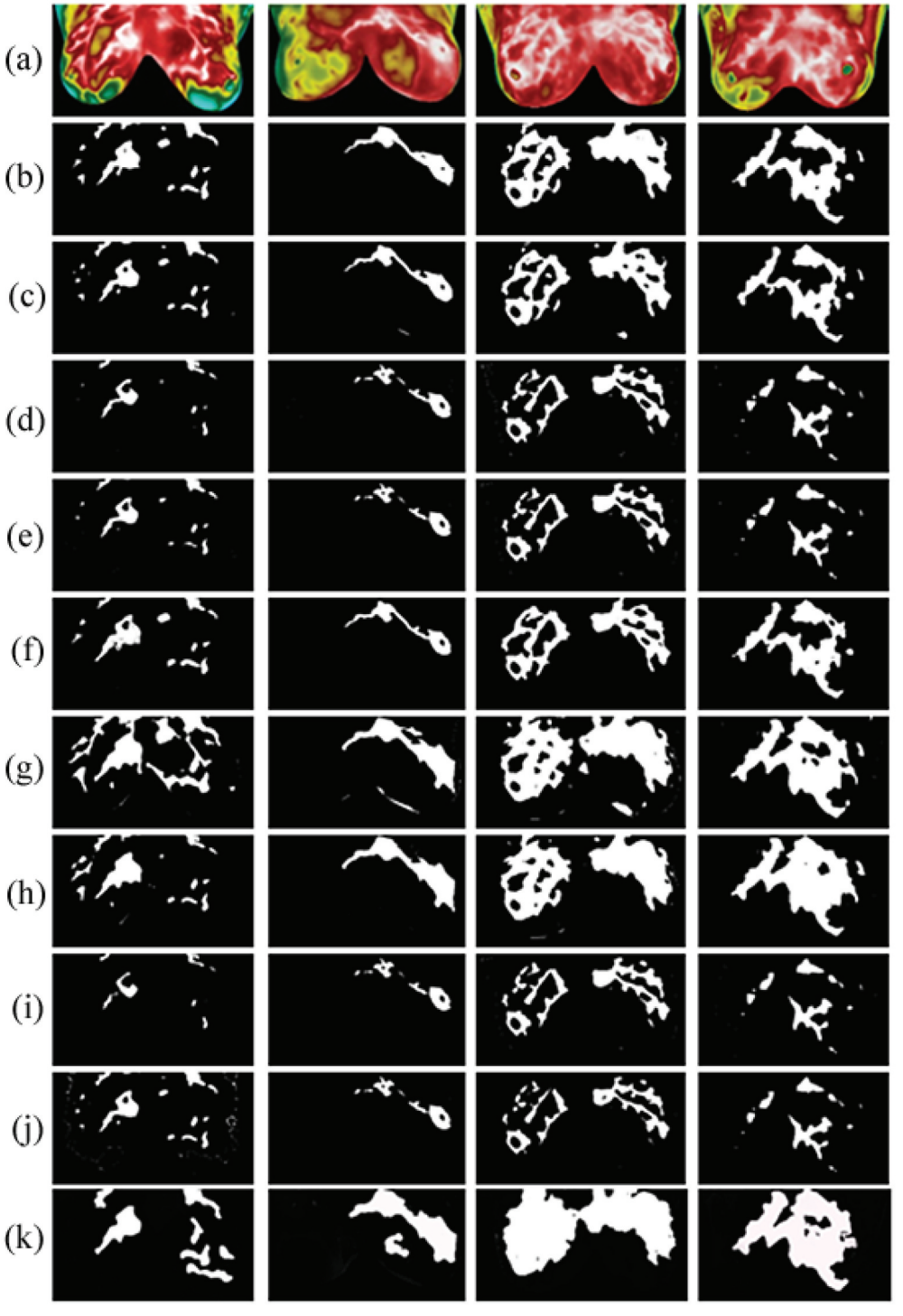

Figure 6. (a) Segmented BRs of some sample breast thermograms, (b) corresponding GT images, segmentation output of (c) proposed segmentation method, (d) KMC, (e) FCM, (f) multi-seeded region growing, (g) FODPSO, (h) MS, (i) expectation maximization, (j) threshold based, and (k) CV level set method.

Table 2. Comparison of state-of-the-art segmentation methods for both DBT-TU-JU and DMR datasets.

	Method Used	DSC	JI	Pr	Re	RMS	OSeg	USeg
DBT-TU-JU Database	The proposed	0.84 ± 0.11	0.75 ± 0.15	0.86 ± 0.13	0.87 ± 0.18	0.12 ± 0.04	0.14 ± 0.13	0.12 ± 0.18
	KMC	0.48 ± 0.17	0.30 ± 0.14	0.37 ± 0.20	0.85 ± 0.27	0.23 ± 0.08	0.63 ± 0.20	0.15 ± 0.27
	FCM	0.50 ± 0.16	0.35 ± 0.14	0.43 ± 0.16	0.81 ± 0.30	0.22 ± 0.06	0.57 ± 0.16	0.19 ± 0.30
	RG	0.65 ± 0.26	0.53 ± 0.25	0.58 ± 0.28	0.85 ± 0.29	0.16 ± 0.05	0.42 ± 0.28	0.15 ± 0.29
	FODPSO	0.67 ± 0.12	0.52 ± 0.13	0.98 ± 0.07	0.52 ± 0.14	0.23 ± 0.05	0.01 ± 0.07	0.47 ± 0.14
	MS	0.59 ± 0.22	0.46 ± 0.21	0.88 ± 0.24	0.48 ± 0.22	0.25 ± 0.09	0.10 ± 0.21	0.50 ± 0.22
	EM	0.44 ± 0.15	0.29 ± 0.12	0.32 ± 0.11	0.88 ± 0.27	0.22 ± 0.06	0.68 ± 0.11	0.12 ± 0.27
	Threshold ($T = 200$)	0.47 ± 0.22	0.33 ± 0.18	0.36 ± 0.21	0.84 ± 0.22	0.20 ± 0.06	0.64 ± 0.21	0.16 ± 0.22
	LS	0.58 ± 0.17	0.43 ± 0.16	0.85 ± 0.19	0.46 ± 0.18	0.27 ± 0.08	0.15 ± 0.19	0.53 ± 0.18
	DLPE-based LS [27]	0.78 ± 0.004	—	—	—	—	—	—
DMR Database	The proposed	0.70 ± 0.17	0.56 ± 0.18	0.62 ± 0.22	0.90 ± 0.16	0.13 ± 0.07	0.38 ± 0.23	0.10 ± 0.17
	KMC	0.38 ± 0.20	0.25 ± 0.16	0.26 ± 0.16	0.86 ± 0.26	0.18 ± 0.08	0.74 ± 0.16	0.14 ± 0.26
	FCM	0.42 ± 0.21	0.29 ± 0.17	0.35 ± 0.16	0.69 ± 0.37	0.20 ± 0.09	0.65 ± 0.16	0.30 ± 0.37
	RG	0.60 ± 0.23	0.46 ± 0.22	0.51 ± 0.25	0.87 ± 0.24	0.15 ± 0.08	0.49 ± 0.25	0.13 ± 0.24
	FODPSO	0.64 ± 0.21	0.50 ± 0.22	0.52 ± 0.23	0.93 ± 0.13	0.14 ± 0.08	0.48 ± 0.22	0.07 ± 0.13
	MS	0.52 ± 0.20	0.45 ± 0.22	0.70 ± 0.25	0.56 ± 0.21	0.27 ± 0.11	0.36 ± 0.25	0.25 ± 0.27
	EM	0.38 ± 0.19	0.25 ± 0.16	0.26 ± 0.15	0.87 ± 0.26	0.18 ± 0.08	0.74 ± 0.15	0.13 ± 0.26
	Threshold ($T = 205$)	0.44 ± 0.22	0.31 ± 0.18	0.33 ± 0.20	0.80 ± 0.21	0.17 ± 0.08	0.67 ± 0.20	0.20 ± 0.21
	LS	0.61 ± 0.19	0.47 ± 0.19	0.80 ± 0.20	0.56 ± 0.22	0.19 ± 0.07	0.19 ± 0.20	0.44 ± 0.22
	RASIT [25]	0.576	—	—	—	—	0.057	0.509
	DLPE-based LS [27]	0.80 ± 0.004	—	—	—	—	—	—

KMC –K means Clustering, RG – Region Growing, FCM – Fuzzy C means, FODPSO - Fractional Order Darwinian Particle Swarm Optimisation, MS – Mean Shift, EM - Expectation Maximisation, LS – Level Set, DLPE - Different local priorities embedded, RASIT - Region shrinking based accurate segmentation of inflammatory areas from thermograms.

produce OSeg results as some necessary regions are discarded as background areas. From Figure 6(f), the segmentation result of RG is also similar to the GT images. Moreover, comparing the results of FDPSO and MS (Figure 6(g–h)) respectively with GT images, FDPSO and MS produce USeg-segmentation results by considering some non-SHRs as SHRs. Similar to KMC and FCM, the EM and threshold-based segmentation methods also produce OSeg results. Additionally, similar to FDPSO and MS, the CV-LS method produces USeg results, as shown in Figure 6(k). Thus, based on the comparison results, the proposed MMSHR is efficient enough for segmenting SHRs.

In addition to the qualitative evaluation, a quantitative evaluation and comparison of the segmentation performance of the proposed method with other state-of-the-art SHRs segmentation methods are provided in Table 2. Here, the mean and variance of all seven segmentation evaluation metrics: DSC, JI, Pr, Re, RMS, OSeg, and USeg are listed. Further, in Table 2, the best metric values are shown in *boldface* for both datasets. As observed, the segmentation performance of the proposed method is better than those of the other methods in terms of all the computed evaluation metrics in both the DBT-TU-JU and DMR datasets. Along with higher mean DSC, JI, Pr and Re values, the lower variance of these metrics indicates the stability of the proposed segmentation method for both datasets. Although the DSC value of the DLPE-based LS [27] for the DMR dataset is better than that of the proposed method, the value of a single metric cannot prove its superiority on the DMR dataset. Moreover, with lower RMS values, the proposed segmentation method proved its efficiency in accurate SHRs segmentation. By comparing the OSeg metric values of all methods, it was found that FDPSO outperforms the proposed method regarding OSeg. However, considering both the OSeg and USeg values, the proposed method outperforms all the state-of-the-art methods.

4.2. Evaluation of degree of severity prediction

This section presents an evaluation of the effectiveness of the proposed MSHRs in terms of the degree of abnormality prediction. The corresponding objective is to quantify the relative contribution of SHRs segmentation and SHRs morphology to the degree of abnormality prediction, in contrast to using image descriptions from the entire BR. To evaluate the classification performance of the proposed MMSHRs system, only statistically significant features were considered. Figure 7 illustrates the boxplots of each feature value computed from each HS_i. To evaluate the statistical significance of these computed features, the Mann-Whitney-Wilcoxon (MWW) test with the significance level 0.001 was employed, and the corresponding *p*-values are shown in Figure 7. As depicted in Figure 7(a–d), the area, *ED* and *FD*of the SA thermograms are considerably larger than those of the MA thermograms. However, the *p*-values ($p < 0.001$) of the above-mentioned features at each HS_i (excluding the area and *ED* of HS_5 and *FDs* of HS_4 and HS_5) prove the efficiency of the three features in differentiating MA thermograms from SA thermograms. Unlike these features, with a *p*-value <0.001, the *CA* of only HS_1 was found to be statistically significant in differentiating the MA thermograms from the SA thermograms. Likewise, the feature value distributions of the RSA computed from the MA and SA thermograms (Figure 7(e)) also indicates that the MA thermograms have significantly smaller ($p < 0.001$) RSA compared with the SA thermograms. To discard the

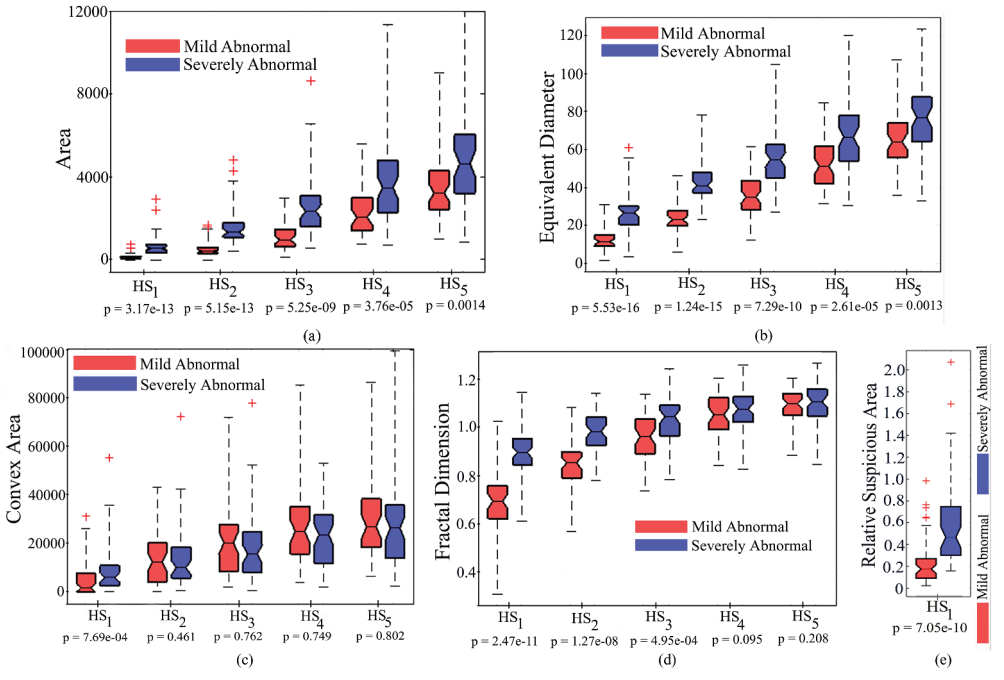

Figure 7. Box plots exhibiting the distribution of feature values of (a) area, (b) ED, (c) CA, (d) FD and (e) RSA obtained from both MA and SA. The p-values obtained for each feature using the MWW test is also specified alongside the corresponding each feature.

redundant features, the relationship between the statistically significant features ($p < 0.001$) was explored across the MA and SA thermograms by doing a correlation analysis. A pictorial representation of the correlation values between the statistically significant features of the MA and SA is demonstrated in Figure 8. As observed, all statistically significant features of both MA and SA are weakly correlated with each other, hence, all these 13 statistically significant features were fed to the SVM classifier, and five-fold cross-validation was employed. The classification performance of the proposed model using SVM with three different kernels is presented in Figure 9. As observed among the three kernels, SVM_R provided the highest classification accuracy. The PPV and NPV of SVM_R were also higher than those of SVM_L and SVM_P. The sensitivity of SVM_P and SVM_R were the same. Similarly, the specificities of SVM_L and SVM_R were the same. However, considering the values of all five-evaluation metrics, SVM_R yielded the highest classification performance.

Moreover, to determine the effectiveness of the proposed MMSHRs over the other methods, this section presents a comparative study. However, due to the absence of a degree of abnormality prediction system in the literature, the authors considered three different sets of features for comparison: first-order statistical (FOS) [13,28], grey level co-occurrence matrix (GLCM) [13,14,30,42], run-length (RL) [42] features as follows. The singular value (SV) used in [11] was also considered for comparison.

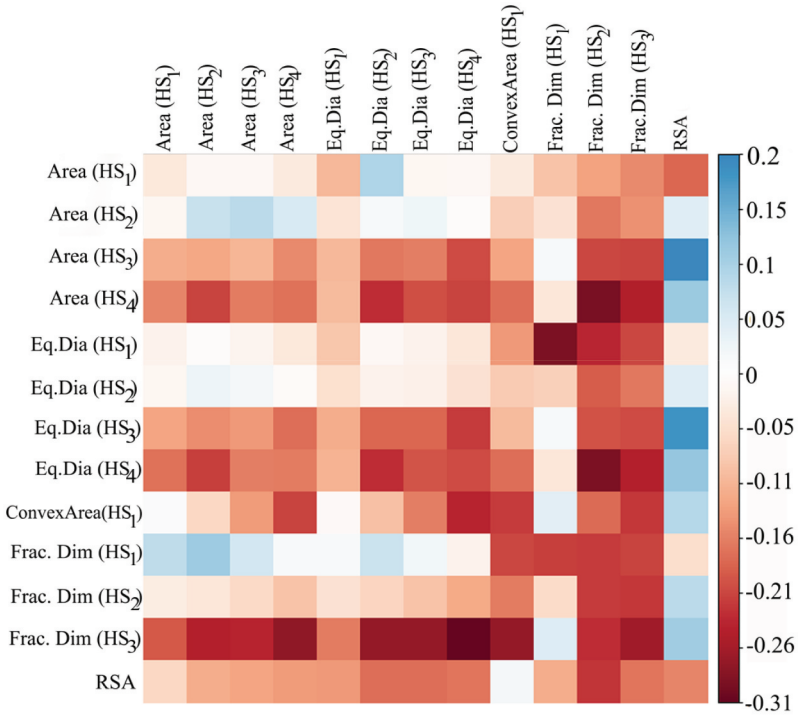

Figure 8. Correlation among statistically significant features between MA and SA groups.

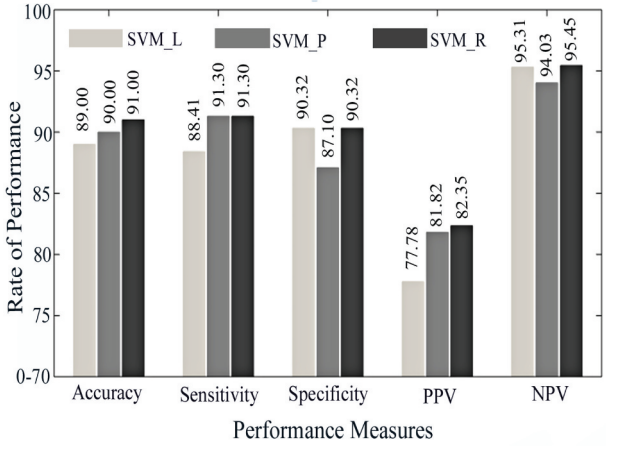

Figure 9. Classification performance of the proposed MMSHRs system in breast abnormality detection.

(1) *FOS features*: the FOS feature set contained six features: mean, skewness, entropy, kurtosis, standard deviation, and variance
(2) *GLCM features*: The GLCM feature set contained 17 features including angular second moment, contrast, correlation, dissimilarity, sum of squares (variance), entropy, homogeneity, inverse difference moment, inverse difference

moment normalised, sum average, sum variance, autocorrelation, sum entropy, difference variance, difference entropy, information measures of correlation 1 and 2 from the co-occurrence matrices. The GLCM features were computed in all four directions (0°, 45°, 90° and 135°) and the averages of feature values in all four directions were considered for comparison.

(3) RL features: The RL feature set comprised 11 features including short-run emphasis, long-run emphasis, grey-level non-uniformity, run-length nonuniformity, run percentage, high grey-level run emphasis, low grey-level run emphasis, short-run low grey-level emphasis, short-run high grey-level emphasis, long-run low grey-level emphasis and long-run high grey-level emphasis. These features were computed in all four directions (0°, 45°, 90° and 135°) and the average of feature values in all four directions were considered for comparison.

(4) Singular values: As described in [11], the SV feature set contains the breast abnormality grading (BAG) index value, which is computed by summing the first two singular values computed from each thermogram.

For an adequate comparison, the features were extracted in two manners, without and with SHRs segmentation. For the case without SHRs segmentation, the left and right breasts were separated from the segmented BRs, as shown in Figure 10. The abovementioned features were then computed by computing the bilateral feature difference between the left and right breasts. Details on the feature extraction without SHRs segmentation are provided in [31]. For the case with SHRs segmentation, features were extracted only from the segmented SHRs. The classification performances of these extracted features were then evaluated using SVM with all three kernels. Note that for comparison, the authors considered only kernels with which each feature set provides the best performance.

As illustrated in Figure 11, among all the feature sets extracted from the entire BRs or from the segmented SHRs, the proposed MMSHRs system provides the best classification accuracy. However, by comparing the classification performance of different features with and without SHRs segmentation, it was observed that except for the SV feature set, the classification performance of the other three feature sets FOS, GLCM and, RL are better when extracted from the segmented SHRs. In addition to the accuracy, the receiver operating characteristic (ROC) curve for each feature set with the SVM classifier is plotted as in Figure 12 for comparison. Similar to other performance measures, the area under the

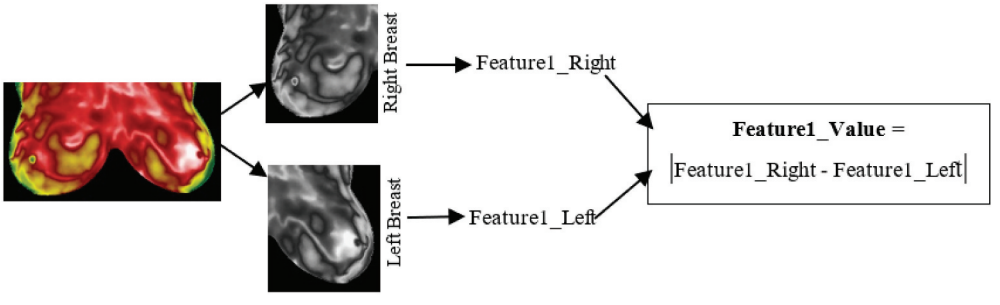

Figure 10. Extraction of feature values from breast thermograms in the case without SHRs segmentation.

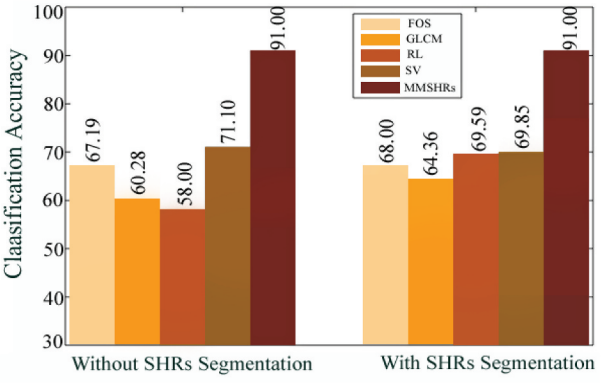

Figure 11. Comparison of classification performance of the proposed MMSHRs with other state-of-the-art feature sets.

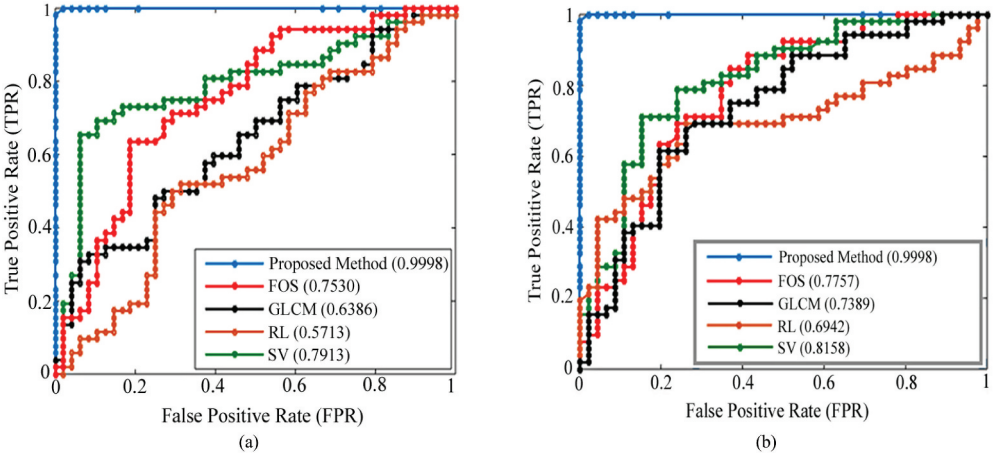

Figure 12. The ROC curves of each feature set obtained (a) with SHRs segmentation and (b) without SHRs segmentation.

ROC curve (AUC) further proves that the proposed system outperforms other feature sets. As depicted in Figures 12(a,b), the AUC of the MMSHRs is considerably better than those of the other four sets of features, whether extracted with or without SHRs segmentation. Thus, the proposed method outperforms other widely used feature sets.

5. Discussion

The proposed MMSHRs system relies on the morphology of SHRs, for which the accurate segmentation of SHRs is crucial. Considering this, an efficient SHRs segmentation method was developed followed by the morphological analysis of the segmented SHRs. This section discusses the advantages and limitations of the proposed MMSHRs system.

5.1. Addresses the limitations of infrared breast thermograms

As described in Section 3, the proposed segmentation method generates an ICM for each thermogram, where each entry in the map is the similarity score of the intensity value of each pixel with the highest intensity value. While computing the similarity score of all pixels in a thermogram, it was noticed that irrespective of the location and shape of SHRs, the similarity score of the pixels in SHRs was higher than that of the pixels in non-SHRs. Hence, based on the similarity score values, it is possible to extract SHRs from anywhere within a BR. Thus, the proposed segmentation method prevents missed segmentation.

5.2. Minimisation of parameter selection

Unlike other state-of-the-art methods, the proposed SHRs segmentation method minimises parameter selection. In clustering-based segmentation techniques, the selection of an optimal cluster is very challenging. Moreover, the segmentation results vary with different cluster numbers. To obtain better accuracy in segmentation, the I-index was used for optimal cluster selection and then, compared the results. Similar to clustering techniques, in RG, a seed point is necessary to start the segmentation and a threshold value must be set to stop the iteration. Further, in deformable model-based segmentation methods, the initial contour should be selected to start the segmentation process for which the locations of the SHRs should be known prior to the segmentation. Moreover, prior to segmentation, the number of iterations must be provided to stop the iteration. Because, the segmentation output depends on the number of iterations, providing an optimal number of iterations is difficult. In contrast, the proposed segmentation method requires only one threshold value (in Otsu's Thresholding technique) to produce the binary segmentation results. Although the number of parameters in the threshold-based segmentation method and the proposed method is same, the accuracy of the proposed segmentation method is considerably higher than that of the threshold-based segmentation method, as shown in Table 2.

5.3. Minimisation of under and over segmentation

As illustrated in Table 2 for both the DBT-TU-JU and DMR datasets, LS and MS overcome the drawback of OSeg at the cost of very high USeg. In contrast, KMC, FCM, RG, EM, and thresholding methods result in low USeg values but very high OSeg values. Considering both of these parameter values to measure the accuracy of segmentation, the proposed segmentation method outperforms the others as minimal OSeg and USeg values are produced in combination.

5.4. Improves SHRs segmentation accuracy

To extract efficient morphological features of SHRs and grade the degree of abnormality in breast thermograms, it is imperative to accurately segment SHRs. From the comparison of the segmented SHRs with the GT images (i.e. Figure 6 in Section 3), the proposed

segmentation method can extract SHRs more accurately than other state-of-the-art methods. Similarly, the quantitative comparison also proves the superiority of the proposed segmentation method over the eight state-of-the-art methods reported in other studies. As shown in Table 2 the higher mean DSC, JI, Pr and Re values and the lower variance of these metrics indicate the stability of the proposed segmentation method for both the DBT-TU-JU and DMR datasets.

5.5. Improves classification accuracy

While designing a CAD system for disease diagnosis, obtaining better accuracy is the key objective. Accordingly, instead of using the features of entire breasts, the morphological features of SHRs were utilised to grade the degree of abnormality in breast thermograms. As depicted in Figure 11, the morphological feature provides better classification accuracy than other state-of-the-art features. Moreover, as shown in Figure 11, in comparison to features extracted without SHRs segmentation, the features extracted from the segmented SHRs provide better classification accuracy.

5.6. Limitations

Because of the difficulty in visualising temperature differences in thermograms, IBT uses pseudo-colours to represent temperature variations across a region of interest. In such representation, brighter colours like white, yellow, and red indicate higher temperatures, whereas darker colours such as purple, dark blue, and black indicate cooler temperatures. To represent thermal emission, different pallets with various pseudo-colours are used in IBT, among which the 'Rainbow HC' colour palette was employed in this work to visualise the temperature difference. Therefore, the performance of the proposed segmentation method may vary if applied to different palettes of pseudo-colours to represent breast thermograms. Consequently, the performance of the degree of abnormality may also vary for different palettes of pseudo-colours.

6. Conclusion

The appearance of SHRs in breast thermograms is the most common marker of breast abnormalities. Accurate segmentation and analysis of SHRs are crucial for grading the severity of breast thermograms, which may assist the radiologists in the early diagnosis of breast disease. However, due to the limitations of breast thermograms, the accurate segmentation of SHRs is challenging; hence, analysis of SHRs for predicting the degree of severity may result in erroneous conclusions. Therefore, this study developed the MMSHRs; the first stage of MMSHRs involved a novel segmentation method based on thermal image characteristics for precisely segmenting the SHRs and in the second phase, morphological analysis of the segmented SHRs was performed to grade the degree of severity. The notable contributions of this study are as follows.

(1) *Segmentation of SHRs*: An SHR segmentation method based on similarity scoring was proposed to effectively handle the issues associated with the segmentation of SHRs.

(2) *Extensive evaluation of the proposed SHRs segmentation method*: An extensive evaluation of the proposed SHRs segmentation method with other state-of-the-art image segmentation methods was performed. The results prove the efficiency of the proposed method in the accurate delineation of SHRs in abnormal breast thermograms.
(3) *Design of a novel breast abnormality grading system based on the morphology of segmented SHRs*: A morphological analysis of extracted SHRs was performed to predict the degree of severity in abnormal breast thermograms. The experimental results show that the proposed MMSHRs system is potential enough to predict the degree of severity.

The proposed segmentation method achieved segmentation of SHRs with significant accuracy. The qualitative and quantitative comparison results of the proposed segmentation method with other state-of-the-art segmentation methods reveal that the proposed method is efficient and stable enough for segmenting SHRs. In the second phase of the proposed MMSHRs system, a set of 13 statistically significant morphological features was considered for grading the degree of severity in breast thermograms. The highest classification accuracy of 91% with a sensitivity of 91.30% and specificity of 90.32% was obtained with the SVM_R classifier. Moreover, from the comparison of the classification performance of the proposed MMSHRs system with those of other state-of-the-art feature sets, the proposed system provides the best classification accuracy among all the feature sets extracted from entire BRs or from segmented SHRs. Designing such a non-invasive type and non-radiating imaging-based breast abnormality grading system will help the remote population to undergo routine breast screening, and if any abnormality is detected, they can seek medical attention for further evaluation of their breast health. This may contribute to lowering the mortality rate of patients with breast cancer.

Although it is evident that the proposed MMSHRs system can assist the physicians in making accurate and early diagnostic decisions to save lives, in future by the expansion of the training set to a large extent the authors can further confirm the strength and limitations of the proposed MMSHRs system. Moreover, a major breakthrough in medical image analysis is the emergence of a deep convolution neural network that can extract small bits of information from large datasets. Therefore, the application of these algorithms to breast thermograms is the goal of future work, which may help in achieving higher classification accuracy.

Acknowledgement

The work presented herein was being conducted at the Bio-Medical Infrared Image Processing Laboratory (BMIRD) of the Computer Science and Engineering Department, Tripura University (A Central University), Suryamaninagar-799022, Tripura (W). The Authors are grateful to Department of Biotechnology (DBT), Government of India, for their support, Government of India for providing a Junior Research Fellowship (JRF) under the DST INSPIRE fellowship program (No. IF150970).

Disclosure statement

All authors declare that they do not have any conflict of interest.

Funding

This work was supported with Grant No. BT/533/NE/TBP/2013, Dated 03/03/2014 from the Department of Biotechnology (DBT), Government of India.

ORCID

Mrinal Kanti Bhowmik http://orcid.org/0000-0002-3194-3656

Data availability statement

The DMR dataset is available at: https://doi.org/10.1080/17686733.2022.2097614.

The DBT-TU-JU dataset: Not publicly available.

Ethics approval/human subjects protections

This work is done by maintaining the ethical standards of AGMC with IRB approval number F.4 (5–2)/AGMC/Academic/Project/Research/2007/Sub-I/8199–8201 dated 18 November 2013.

References

[1] Madhavi V, Thomas CB. Multi-view breast thermogram analysis by fusing texture features. Quant Infrared Thermogr J. 2019;16(1):111–128.
[2] National Cancer Institute: SEER Stat Fact Sheets: Breasts. Available from:www.seer.cancer.gov/statfacts/html/breast.html
[3] Breast Cancer India: Pink Indian statistics. Available from: http://www.breastcancerindia.net/bc/statistics/stat_global.htm
[4] Gogoi UR, Bhowmik MK, and Bhattacharjee D. A study and analysis of hybrid intelligent techniques for breast cancer detection using breast thermograms. In: Bhattacharyya S, Dutta P, Chakraborty S C, et al., editors. Hybrid soft computing approaches. New Delhi: Springer; 2016. p. 329–359.
[5] Chebbah NK, Ouslim M, Benabid S. New computer aided diagnostic system using deep neural network and SVM to detect breast cancer in thermography. Quant Infrared Thermogr J. 2022;1–16. DOI:10.1080/17686733.2021.2025018
[6] Josephine Selle J, Shenbagavalli A, Sriraam N, et al. Automated recognition of ROIs for breast thermograms of lateral view-a pilot study. Quant Infrared Thermogr J. 2018;15(2):194–213.
[7] Kennedy DA, Lee T, Seely D. A comparative review of thermography as a breast cancer screening technique. Integr Cancer Ther. 2009;8(1):9–16.
[8] Mahmoudzadeh E, Montazeri MA, Zekri M, et al. Extended hidden Markov model for optimized segmentation of breast thermography images. Infrared Phys Technol. 2015;72:19–28.
[9] Kirubha AS, Anburajan M, Venkataraman B, et al. Comparison of PET–CT and thermography with breast biopsy in evaluation of breast cancer: a case study. Infrared Phys Technol. 2015;73:115–125.
[10] Kwok J, Krzyspiak J. Thermal imaging and analysis for breast tumor detection. Computer-Aided Eng. 2007;453.
[11] Gogoi UR, Bhowmik MK, Bhattacharjee D, et al. Singular value based characterization and analysis of thermal patches for early breast abnormality detection. Aus Phys Eng Sci Med. 2018;41(4):861–879.
[12] Raghavendra U, Gudigar A, Rao TN, et al. Computer-Aided diagnosis for the identification of breast cancer using thermogram images: a comprehensive review. Infrared Phys Technol. 2019;102:103041.

[13] Hakim AS, Awale RN. Extraction of hottest blood vessels from breast thermograms using state-of-the-art image segmentation methods. Quant Infrared Thermogr J. 2021;1–19. DOI:10.1080/17686733.2021.1974209
[14] Roslidar R, Rahman A, Muharar R, et al. A review on recent progress in thermal imaging and deep learning approaches for breast cancer detection. IEEE Access. 2020;8:116176–116194.
[15] Etehad Tavakol M, Chandran V, Ng EYK, et al. Breast cancer detection from thermal images using bispectral invariant features. Int J Ther Sci. 2013;69:21–36.
[16] Francis SV, Sasikala M, Saranya S. Detection of breast abnormality from thermograms using curvelet transform based feature extraction. J Med Syst. 2014;38(4):23.
[17] Golestani N, Etehad Tavakol M, Ng EYK. Level set method for segmentation of infrared breast thermograms. Excli J. 2014;13:241.
[18] Etehad Tavakol M, Sadri S, Ng EYK. Application of K-and fuzzy c-means for color segmentation of thermal infrared breast images. J Med Syst. 2010;34(1):35–42.
[19] Prakash RM, Bhuvaneshwari K, and Divya M, et al. Segmentation of thermal infrared breast images using K-means, FCM and EM algorithms for breast cancer detection. In: 2017 international conference on innovations in information, embedded and communication Systems (ICIIECS); 2017 March 17; Coimbatore, India; IEEE; 2017. p. 1–4.
[20] Etehadtavakol M, Ng E, and Lucas C. Fuzzy C means segmentation and fractal analysis of the benign and malignant breast thermograms. In: Diakides M, Bronzino J D, Peterson D R, et al., editors . Medical Infrared Imaging.CRC Press; 2012. 16-1– 16–20.
[21] Sayed GI, Soliman M, and Hassanien AE. Bio-Inspired swarm techniques for thermogram breast cancer detection. In: Dey N, Bhateja V, Hassanien A E, editors.Medical imaging in clinical applications. Cham: Springer; 2016. p. 487–506.
[22] Milosevic M, Jankovic D, Peulic A. Thermography based breast cancer detection using texture features and minimum variance quantization. Excli J. 2014;13:1204.
[23] Shahari S, and Wakankar A. Color analysis of thermograms for breast cancer detection. In: 2015 international conference on industrial instrumentation and control (ICIC); 2015 May 28; Pune, India: IEEE; 2015. p. 1577–1581.
[24] Wakankar AT, Suresh GR. Automatic diagnosis of breast cancer using thermographic color analysis and SVM classifier. In: The International Symposium on Intelligent Systems Technologies and Applications. Cham: Springer; 2016. p. 21–32.
[25] Etehadtavakol M, Emrani Z, Ng EYK. Rapid extraction of the hottest or coldest regions of medical thermographic images. Med Biol Eng Comput. 2019;57(2):379–388.
[26] Lavanya A. An approach to identify lesion in infrared breast thermography images using segmentation and fractal analysis. Int J Biomed Eng Technol. 2015;19(3):220–229.
[27] Pramanik S, Banik D, and Bhattacharjee D, et al. Suspicious-Region segmentation from breast thermogram using DLPE-based level set method. IEEE Trans Med Imaging. 2018;38 (2):572–584.
[28] Bardhan S, Bhowmik MK, Debnath T, et al. RASIT: region shrinking based accurate segmentation of inflammatory areas from thermograms. Biocybern Biomed Eng. 2018;38 (4):903–917.
[29] Bhowmik MK, Gogoi UR, Majumdar G, et al. Designing of ground-truth-annotated DBT-TU-JU breast thermogram database toward early abnormality prediction. IEEE J Biomed Health Inform. 2017;22(4):1238–1249.
[30] Silva LF, Saade DCM, Sequeiros GO, et al. A new database for breast research with infrared image. J Med Imaging Health Inform. 2014;4(1):92–100.
[31] Gogoi UR, Bhowmik MK, and Ghosh AK, et al. Discriminative feature selection for breast abnormality detection and accurate classification of thermograms. In: IEEE international conference international conference on innovations in electronics, signal processing and communication (IESC); Shillong, India; 2017. p. 39–44.
[32] Otsu N. A threshold selection method from gray-level histograms. IEEE Trans Syst Man Cybern. 1979;9(1):62–66.
[33] Falconer K. Fractal geometry: mathematical foundations and applications. New York: Wiley; 2004.

[34] Backes AR, Bruno OM. Medical image retrieval based on complexity analysis. Mach Vision Appl. 2010;21(3):217–227.
[35] Vapnik VN. The nature of statistical learning theory. NewYork, NY: Springer; 1995.
[36] Brosch T, Tang LYW, Yoo Y, et al. Deep 3D convolutional encoder networks with shortcuts for multiscale feature integration applied to multiple sclerosis lesion segmen-tation. IEEE Trans Med Imaging. 2016;35(5):1229–1239.
[37] Pont-Tuset J, Marques F. Supervised evaluation of image segmentation and object proposal technique. IEEE Trans Pattern Anal Mach Intell. 2016;38(7):1465–1478.
[38] Xu J, Xiang L, Liu Q, et al. Stacked sparse autoencoder (SSAE) for nuclei detection on Breast Cancer Histopathology images. IEEE Trans Med Imaging. 2016;35(1):119–130. DOI:10.1109/TMI.2015.2458702
[39] Hosseini MP, Nazem-zadeh MR, Pompili D, et al. Comparative performance evaluation of automated segmentation methods of hippocampus from magnetic resonance images of temporal lobe epilepsy patients. Med Phys. 2016;43(1):538–553.
[40] Belgiu M, Dragut L. Comparing supervised and unsupervised multiresolution segmentation approaches for extracting buildings from very high resolution imagery. ISPRS J Photogramm Remote Sens. 2014;96:67–75.
[41] Maulik U, Bandyopadhyay S. Performance evaluation of some clustering algorithms and validity indices. IEEE Trans Pattern Anal Mach Intell. 2002;24(12):1650–1654.
[42] Acharya UR, Ng EYK, Tan JH, et al. Thermography based breast cancer detection using texture features and support vector machine. J Med Syst. 2012;36(3):1503–1510.